The Timing of Endocytosis after Activation of a G-Protein-Coupled Receptor in a Sensory Neuron

Lie-Cheng Wang,*†‡ Wei Xiong,*† Jing Zheng,† Yang Zhou,† Hui Zheng,*† Chen Zhang,*† Liang-Hong Zheng,*†
Xue-Liang Zhu,§ Zhi-Qi Xiong,† Lu-Yang Wang,*¶ He-Ping Cheng,*‖ and Zhuan Zhou*†‖

*Institute of Molecular Medicine, Peking University, Beijing, China; †Institute of Neuroscience, Shanghai Institutes for Biological Sciences,
Chinese Academy of Sciences, Shanghai, China; ‡Department of Physiology, Anhui Medical University, Hefei; China; §Institute of
Biochemistry and Cell Biology, Shanghai Institutes for Biological Sciences, Chinese Academy of Sciences, Shanghai, China; ¶Program in
Brain and Behavioral Research & Division of Neurology, The Hospital for Sick Children and Department of Physiology, University of Toronto,
Toronto, Canada; and ‖State Key Laboratory of Biomembrane Engineering, College of Life Sciences, Peking University, Beijing, China

ABSTRACT   Endocytosis is a fundamental cellular event in membrane retrieval after exocytosis and in the regulation of receptor-mediated signal transduction. In contrast to the well-studied depolarization-induced membrane recycling, little is known about the kinetics of ligand-induced endocytosis of G-protein-coupled receptors in neurons. Here we investigated the kinetics of ligand-receptor binding-induced endocytosis in rat sensory neurons using a membrane capacitance assay. The time constant of ADP-induced endocytosis of P2Y-receptors was determined as 1.7 s. The ADP-induced endocytosis was blocked by antagonists against P2Y, phosphorylation, and clathrin. However, block of dynamin was without effect. The ADP-induced endocytosis was confirmed independently by a single vesicle image technique using a styryl FM2-10. Finally, the receptors were internalized in response to ADP, as determined by GFP-labeled P2Y. We conclude that ligand-receptor binding leads to rapid endocytosis in the cytoplasm of rat dorsal root ganglion neurons.

INTRODUCTION

After an action potential, the timing of Ca^{2+}-dependent exocytosis is responsible for rapid (<1 ms) neurotransmission, which sets a theoretical time limit on responses to stimuli (1,2). Neurotransmitters released from a presynaptic cell bind to postsynaptic receptors, including ligand-gated ion channels and G-protein-coupled receptors (GPCRs). The latter represent the largest superfamily of receptor proteins for transmembrane signaling (3–5). This ligand-receptor binding (LRB) is usually followed by a process known as endocytosis or receptor internalization (6–9). Depsite the well-established roles of LRB-induced endocytosis in synaptic plasticity and neuromodulation (6,10,11), and the insulin-induced endocytosis (12–15), real-time temporal dynamics of this process is still obscure.

Endocytosis can be triggered by either preceding exocytosis (10,16,17), or by binding between a chemical ligand and its receptor (5,6). The timing of LRB-induced endocytosis is important because this sets time limits for i), reuse of the desensitized receptors; and ii), intracellular signal transduction. Due to the lack of a real-time assay, most studies of ligand-induced endocytosis had poor time resolution (>2 min). The biochemical experiments used populations of cells and found that cell endocytosis occurs within 2 min after applying ligand (18,19). In brain slices, the long-term depression detected by electrophysiology has been used as an indirect assay for endocytosis before and after ligand application, but the time resolution is >5 min (20).

Membrane capacitance (Cm) has been used as a real-time assay for voltage-induced exocytosis and endocytosis (21,22), and for ligand-induced exocytosis in endocrine cells (23–25). In most neurons, evoked exocytosis and endocytosis were observed not in the soma but in presynaptic terminals, where voltage-clamp and Cm recording are impossible except in a few preparations (26,27). Recently, evoked exocytosis and endocytosis in somata were found in dorsal root ganglion (DRG) neurons (17,28,29). This provides an opportunity to study the temporal kinetics of ligand-induced exocytosis and endocytosis in a neuron using the Cm assay.

In this study, we take advantage of the high time resolution of Cm to resolve endocytosis of GPCRs induced by LRB in small DRG neurons, which contribute to the sense of pain and temperature via neurotransmitters such as ATP and ADP (30). When ADP was applied to a DRG neuron, P2Y-mediated endocytosis occurred with a time constant of 1.7 s. The ADP-induced endocytosis was confirmed by single vesicle imaging using confocal microscopy, as well as by GFP-labeled P2Y experiments, which showed P2Y receptors were internalized after ADP-induced endocytosis. These findings reveal the real-time kinetics of ADP-induced endocytotic vesicles, which may be representative of the kinetics of other endocytotic processes induced by ligand-receptor binding.

MATERIALS AND METHODS

Green fluorescent protein (GFP) labeled P2Y1 plasmid

pGEM3Z-P2Y1 cDNA was kindly provided by Graeme Bell. P2Y1 cDNA was amplified using the polymerase chain reaction with the following primer pairs:

5′-CCGGAATTCATGACCGAGGTGCCTTGG-3′ and 5′-CGCGGAT-CCCGCAAACTTGTGTGTCTCCGTTC-3′. The BamH1/EcoR1 fragment of P2Y1 was subcloned into pEGFP-N1 to generate EGFP-P2Y1 fusion protein.

Cell transfection

Human embryonic kidney (HEK) 293T cells were cultured in DMEM (GIBCO) supplemented with 10% FBS. EGFP-labeled P2Y1 plasmids were introduced into 80% confluent HEK293T cells using the BES-Calcium phosphate transfection protocol as described previously (31). HEK293T cells were used for experiments 36–48 h after transfection. Rat DRG neurons were cultured as previously described (17). EGFP-labeled P2Y1 plasmids were introduced into cultured DRG neurons (2 DIV) by lipofection using the standard reference protocol of Invitrogen (32). Briefly, 0.5 μg DNA per well was added into 25 μl serum-free medium, diluted with 2 μl Lipofectamine and 25 μl medium before adding 0.2 ml serum-free medium at room temperature for 25 min to allow the formation DNA-liposome complexes. These DNA-liposome complexes were incubated with cells for 6 h at 37°C in a CO_2 incubator before changing the medium with normal serum medium. Transfected DRG neurons were used for experiments after 36 h.

Cell preparation and patch clamp recordings

DRG neurons were prepared as previously described (28) and used 1–8 h after preparation. Only small (the C-type) neurons (15–25 μm in diameter) without apparent processes were used. Whole-cell recordings were performed using either an EPC9/2 amplifier and Pulse software (HEKA Elektronik, Lambrecht/Pfalz, Germany), or a PC-2B patch-amplifier (INBIO, Wuhan, China) and Pulse Control 5.0 software (from Richard Bookman, Miami University, Miami, FL) (33) together with an ITC-18 interface (Instrutech, Elmont, New York) for data acquisition. Cells were voltage-clamped at −80 mV with pipettes of 2–4 MΩ resistance. Data were
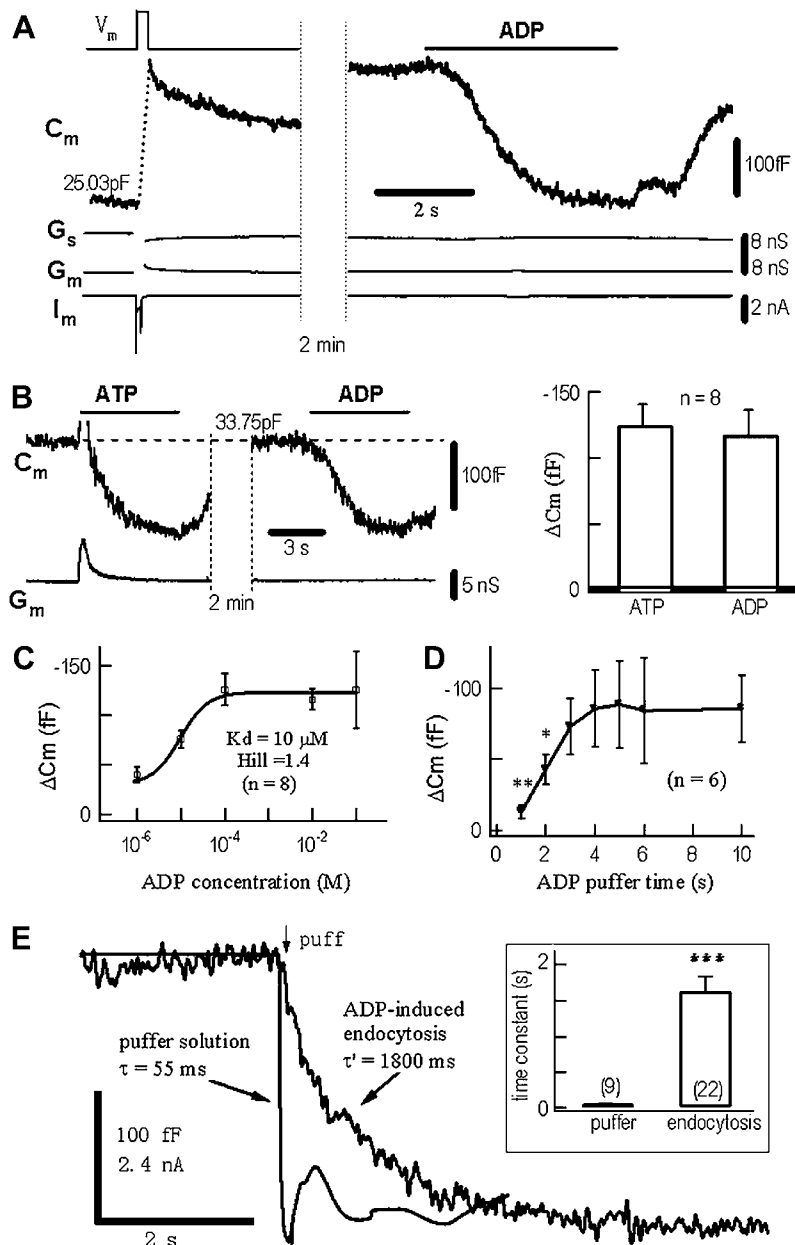
FIGURE 1 Timing of ADP-induced endocytosis in DRG neurons measured by membrane capacitance (Cm). (A) A 200-ms depolarizing pulse (V_m) induced a whole-cell Ca^{2+} current (I_m) and a rapid Cm increase of 280 fF, which represented a normal depolarization-secretion coupling (17,28,29). Subsequently, the cell was stimulated with ADP (0.1 mM) for 5 s, which induced a Cm decrease of −260 fF, which represented a ligand-endocytosis coupling. The changes in Gs and Gm were negligible. Cm recovered partially after washout of ADP. (B) In another neuron, application of either ATP (0.1 mM, left panel) or ADP (0.1 mM, middle panel) induced comparable decreases in Cm (right panel). On average, the 7-s puffs of 0.1 mM ATP and ADP induced Cm signals of −125 ± 16 fF and −118 ± 17 fF, respectively ($n = 8$). Activation of P2X channels by ATP induced a transient inward current (I_m), which caused a transient Cm artifact (the overshooting part of the artifact is clipped). (C) Dose-dependent Cm signals induced by 1 μM–10 mM ADP. The Hill coefficient was 1.4. ADP-induced Cm signals saturated for ADP > 0.1 mM (Kd = 10 μM). The maximum Cm signal was −125 ± 16 fF ($n = 8$). (D) Puff time-dependent Cm signals induced by 0.1 mM ADP. The ADP-induced Cm signal saturated at $t > 3$ s ($n = 6$). (E) Determination of the kinetics of ADP-induced endocytosis. The time constant of the solution exchange was 55 ms (see Methods). After replacing the solution of this puffer channel with 0.1 mM ATP, the ADP-induced endocytosis (total −210 fF) with a time constant of 1.8 s was measured by Cm recording in a DRG neuron. On average, the time constants were 65 ± 7 ms ($n = 9$) and 1.7 ± 0.2 s ($n = 22$) for puffer solution exchange and cell endocytosis, respectively (inset). Times of puff solutions are indicated by the application bars, except panel (E), where the application continued after the onset arrow.

analyzed with Igor Pro software (Wavemetrics, Lake Oswego, OR). Standard external solution (ES) contained (in mM): 150 NaCl, 5 KCl, 2.5 CaCl$_2$, 1 MgCl$_2$, 10 HEPES, 10 glucose, pH 7.4. The intracellular solution contained (in mM): 153 CsCl, 1 MgCl$_2$, 10 HEPES, 4 ATP, pH 7.2. All chemicals were from Sigma (St. Louis, MO), except FM2-10 (Molecular Probes, Eugene, OR).

All experiments were carried out at room temperature (22–25°C), and data were given as mean ± SE. The significance of differences was tested using Student's t-test (*$p < 0.05$, **$p < 0.01$, ***$p < 0.001$).

Rapid solution application

A perfusion system with a fast exchange time by electronic switching between seven channels applied reagents to a cell under study (RCP-2B, INBIO Inc., Wuhan, China; for its kinetic properties see (34)). We determined the speed of our puffer system by measuring the conductance between a patch electrode and the reference electrode. The puffer solution (water) had a low conductance, whereas the bath solution and the patch-pipette solution were standard ES. Before the test, a small holding potential was applied to the patch-pipette to generate a holding current. When water was locally puffed to the patch electrode, the current decreased to a steady state (0 conductance). To reduce contamination and speed up the solution exchange in cell experiments, a patch-clamped cell was puffed with ES immediately before and after application of ADP (or other reagents). Differences in flow speed may cause a flow-dependent capacitance artifact (data not shown). To minimize this flow artifact, the flow speeds of different channels (for ADP, ES, etc.) were checked and adjusted to the same value (0.5 ml/min, with a 5 mm long puffer tip 0.1 mm in diameter). Under these conditions, capacitance artifacts caused by puffer solution exchanges were negligible.

Membrane capacitance measurements

The membrane capacitance was measured using either the software lock-in module of Pulse 8.30 with an EPC9/2 amplifier, or the Pulse Control 5.0 phase-tracking module with a PC-2B amplifier; both give similar capacitance signals (28). A 1 kHz, 40 mV peak-to-peak sinusoid was applied around a DC holding potential of −80 mV. The normalized Cm traces were fitted with a single exponential curve: $F(t) = y_0 + A \times \exp(-t \times \tau^{-1})$, where t is the time after giving ADP and $F(t)$ is the Cm change. Since 0.1 mM ADP induces a maximum endocytosis after 3 s, y_0 represents the ratio of ADP-induced endocytosis to the maximum endocytosis (R_{endo}); τ represents the decay time constant.

## Single vesicle and single cell fluorescence imaging

FM2-10 was loaded into freshly isolated DRG neurons as described previously (17). Briefly, neurons were incubated in 100 μM FM2-10 with or without 0.1 mM ADP for 3 min. Then, cells were washed three times with standard ES (2.5 mM Ca^{2+}) to remove nonspecific FM staining. The confocal images were obtained with 0.08 μm/pixel at 1 Hz. Fluorescent spots in the cell soma were counted using Image-Pro Plus software (Media Cybernetics, Silver Spring, MD). The size and magnification of the picture acquired from the confocal microscope were constant (512 × 512 pixels). The image was first smoothed by a factor of 20 (a function of the software). According to vesicle size, the area range of fluorescent spots was set from 0.04 μm^2 (6 pixel^2) to 1 μm^2 (160 pixel^2).

RESULTS

Timing of a GPCR-induced endocytosis

DRG neurons express two principal types of ATP receptors, P2X and P2Y, which are involved in pain and temperature

transmission (30). The ADP-insensitive P2X is a cation channel, whereas the ADP-sensitive P2Y is a GPCR (35). Under whole-cell recording, a depolarization pulse induced a +280 fF Cm jump, or exocytosis of ~560 dense-core vesicles from the soma of a typical DRG neuron (28)(Fig. 1 A). Subsequently, in the same neuron, 0.1 mM ADP induced a −260 fF Cm jump. Because there were no accompanied changes in the membrane conductance (Gm) and access conductance (Gs), the ADP-induced Cm reduction was presumably due to endocytosis caused by ADP binding to P2Y receptors. The ADP-induced Cm decrease was not dependent on whether there was preceding exocytosis (see below). In the absence of ADP, similar puffs did not cause detectable Cm signals (data not shown). Like 0.1 mM ADP, 0.1 mM ATP induced a similar negative Cm jump (in the presence of P2X activation), indicating that P2Y, but not P2X was primarily responsible for the Cm decrease/endocytosis (Fig. 1 B). The ADP-induced Cm response displayed dose-dependence, with a K$_d$ of 10 μM and Hill
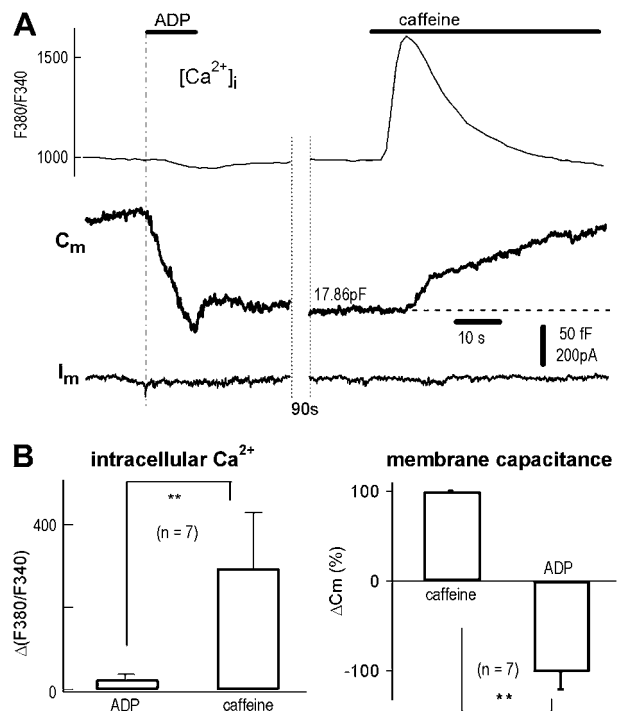
FIGURE 2 ADP-induced endocytosis in the absence of Ca^{2+} influx and Ca^{2+} release from Ca^{2+} stores. (A) With the micro-puffer system for chemical stimulation and Cm recording for exocytosis (Cm increase) and endocytosis (Cm decrease), 0.1 mM ADP induced a rapid endocytosis (−116 fF). Subsequently, 20 mM caffeine induced an exocytosis (+83 fF). Combined [Ca^{2+}]$_i$ imaging showed that caffeine, but not ADP, induced a [Ca^{2+}]$_i$ spike (upper traces). Note, because the dilution in puffer tip (34), Cm reduction signal did not reach its saturation level during the 10 s application. (B) Statistics of experiments using protocols of panel A. [Ca^{2+}]$_i$ measured by changes in F380/F340 (ΔF380/F340) was −25 ± 11 and 290 ± 110 (arbitrary units), corresponding to ADP and caffeine, respectively (left panel). ADP-induced endocytosis (decrease in Cm) was −102 ± 19% of caffeine-induced exocytosis (n = 7, right panel).

coefficient of 1.4 (Fig. 1 C). For low ADP concentrations ($<$ 10 μM), the onset rate of ADP-induced Cm was concentration-dependent. At fixed 0.1 mM ADP, the ADP-induced Cm signal was dependent on application time. The time for 50% of maximum Cm signal was 2 s (Fig. 1 D).

Cm recording of stimulus-endocytosis coupling offers an opportunity to measure the time between the LRB event and the LRB-induced endocytosis. As shown in Fig. 1 E, the onset time constant of the puff system was 55 ms, whereas the time constant of the ADP-induced Cm decrease in the DRG neuron was 1.8 s (average = 1.7 $\pm$ 0.2 s, n = 22). Compared with previous estimates using biochemical (2 min) (18,19) or postsynaptic signals (5 min) (6), the time resolution of ligand-induced endocytosis recordings was remarkably improved by the Cm measurements.

ADP-induced endocytosis without increasing [Ca^{2+}]$_i$

In many cells, endocytosis requires a increase in Ca^{2+} (8,36). In DRG neurons, however, a rapid endocytosis follows the Ca^{2+}-independent but voltage-dependent secretion, termed

CIVDS-RE, which is itself Ca^{2+}-independent (17). We therefore examined the possible involvement of Ca^{2+} influx and Ca^{2+} stores in the ADP-induced endocytosis. Cm was combined with rapid drug exchange to record ligand-induced exocytosis and endocytosis in single DRG neurons (Fig. 2 A, left). Using combined [Ca^{2+}]$_i$ and whole-cell recording, a 10-s puff of 0.1 mM ADP induced no [Ca^{2+}]$_i$ spike but did evoke an endocytosis or negative Cm jump (-136 fF). In contrast, a subsequent puff of 20 mM caffeine, a membrane-permeable ligand of the ryanodine receptor channel for ER Ca^{2+} stores, induced a large [Ca^{2+}]$_i$ spike as well as a Ca^{2+}-dependent exocytosis or positive Cm jump ($+83$ fF) (Fig. 2 A, right). In seven cells, the caffeine-induced Cm increase/exocytosis was significantly different from ADP-induced Cm decrease/endocytosis ($p < 0.01$, Fig. 2 B). Note the two Cm signals were opposite in polarity. The difference between [Ca^{2+}]$_i$ in response to ADP and caffeine are also statistically different ($p < 0.01$). These experiments demonstrate that, unlike exocytosis triggered by caffeine, endocytosis induced by ADP occurs without a measurable increase in [Ca^{2+}]$_i$ (which does not exclude an undetectable local [Ca^{2+}]$_i$ transient).
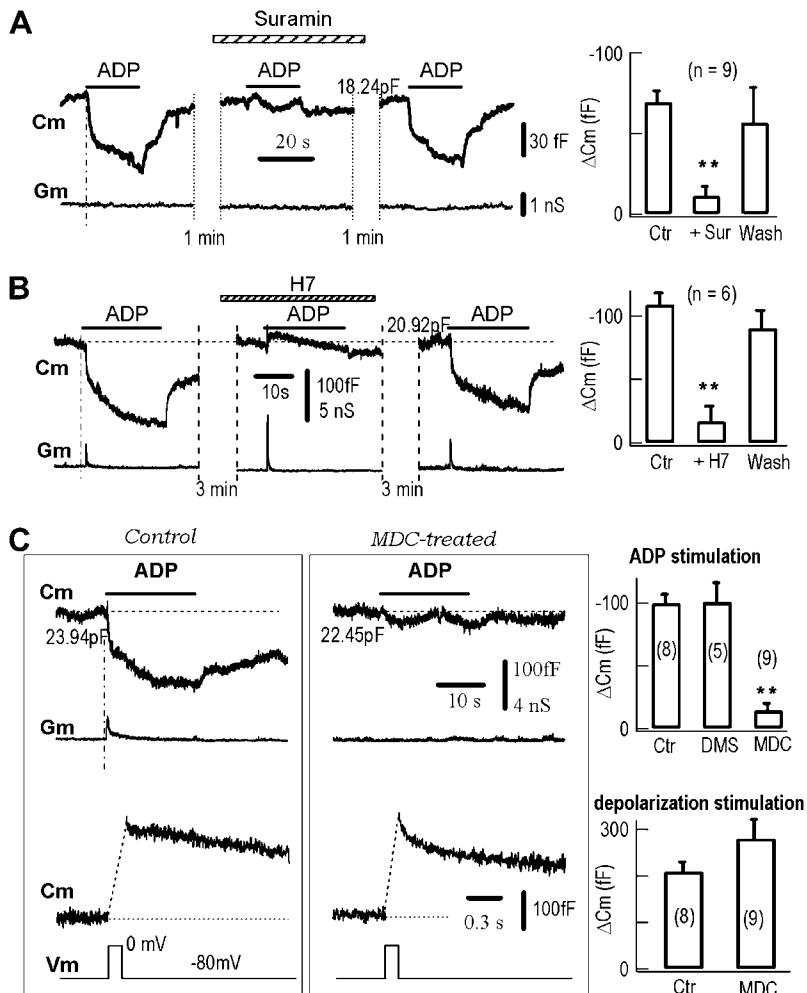
FIGURE 3 Block of ADP-induced endocytosis by antagonists against the ADP receptor, phosphorylation and clathrin. (A) Suramin (0.1 mM) reversibly blocked ADP-induced endocytosis/Cm signals in a representative neuron (left). Statistically, ADP-induced Cm signals were -69 ± 6 fF, -11 ± 5 fF and -57 ± 20 fF for control, suramin and wash, respectively ($n = 9$, right). (B) H7 (0.1 mM) reversibly blocked ADP-induced endocytosis/Cm signals in another representative neuron (left). Statistically, ADP-induced Cm signals were -109 ± 9 fF, -17 ± 12 fF and -91 ± 11 fF for control, H7, and wash, respectively ($n = 6$, right). (C) MDC irreversibly blocked ADP-induced endocytosis but not depolarization-induced exocytosis. ADP-induced Cm signals were irreversibly blocked by MDC (0.1 mM MDC + 0.2% DMSO, 1 h preincubation) (upper traces). In contrast, the depolarization-induced exocytosis/Cm signals were unaffected by MDC (lower traces). The control neuron (left panels) and the MDC-treated neuron (middle panels) were from the same batch. Statistically, ADP-induced Cm signals were -100 ± 7 fF, -101 ± 15 fF, and -15 ± 5 fF for control ($n = 8$), 0.2% DMSO ($n = 5$), and MDC-treated cells ($n = 9$), respectively (upper right). The depolarization (Vm from -80 mV to 0 mV for 200 ms)-induced Cm signals were 209 ± 19 fF, and 290 ± 39 fF for control ($n = 8$) and MDC-treated cells ($n = 9$), respectively (lower right).

Signal pathway involved in ADP-induced endocytosis

The signal transduction pathway of ligand-induced endocytosis includes the receptor, phosphorylation (20,37), and clathrin (38). Suramin, an antagonist against ATP receptors (35), reversibly blocked ADP-induced Cm signals (Fig. 3 *A*), confirming that the endocytotic signals were mediated by P2Y receptors. Further, H-7, a nonspecific antagonist of protein phosphorylation, reversibly blocked the ADP-induced Cm signals (Fig. 3 *B*). This result is consistent with the previous finding that LRB-induced endocytosis is dependent on protein phosphorylation (20). Finally, we tested the effect of monodansylcadaverine (MDC), an antagonist of transglutaminase, a membrane-bound enzyme that actively participates in receptor-mediated and clathrin-dependent endocytosis (38). In neurons treated with 0.1 mM MDC for 1 h, the ADP-induced endocytotic Cm signals were completely suppressed, whereas the depolarization-induced exocytotic Cm signals remained intact in the same neurons (Fig. 3 *C*). Taken

together, these data suggest that ADP-induced endocytosis uses the signal pathway responsible for receptor internalization.

Dynamin is a small GTPase protein, which is required for endocytosis in many neurons (39–41). It is known that the depolarization-induced slow endocytosis, as detected by the Cm decrease after depolarization-induced Cm signals, is dependent on both Ca^{2+} and dynamin (17,42–44). In control DRG neurons, the endocytosis/Cm decay after a depolarization-induced Cm jump/exocytosis was intact after 11 min whole-cell dialysis (data not shown). Intracellular dialysis of 0.25 mg/ml dynPRD, which is a peptide of mutant dyanmin-1, blocked the Ca^{2+}-dependent slow endocytosis (Fig. 4 *A*, *upper panels*, see also (17,43)). However, ADP-induced endocytosis was intact even after 16 min of whole-cell dialysis of dynPRD (Fig. 4 *A*, *lower panels*), indicating that ADP-induced endocytosis is insensitive to dynamin-1.

In chromaffin cells, in addition to dynamin-1 dependent endocytosis, there is a dynamin-2 dependent endocytosis (45). Both dynamin-1 and dynamin-2 are GTPases and require
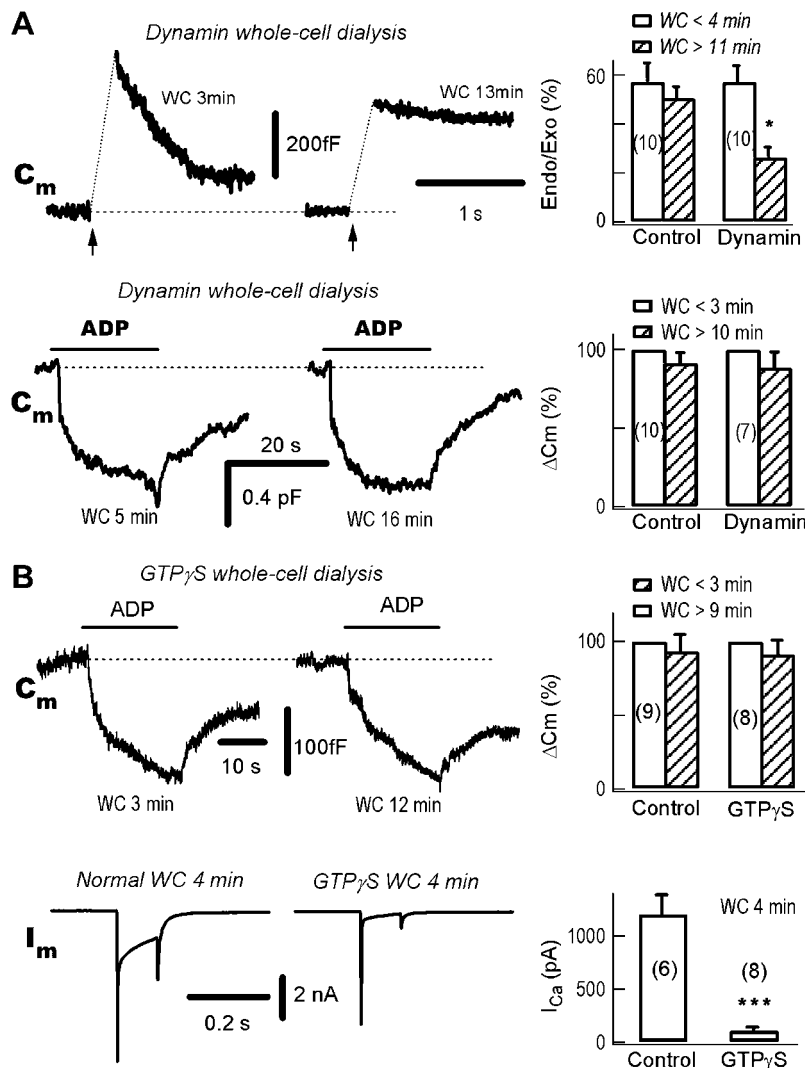
FIGURE 4 The ADP-induced endocytosis is dynamin-independent. (*A*) ADP-induced endocytosis is independent of dynamin-1. In the same neuron, the left panels show a typical experiment during whole-cell (WC) dialysis of the mutant dynamin-1 dynPRD (250 μg/ml). The neuron was stimulated either by depolarizing pulses (*upper traces*) or ADP puffs (*lower traces*) at the times indicated. The exocytosis-coupled endocytosis was substantially blocked at 13 vs. 3 min. (*Upper right*) Statistically, the pulse-induced endocytosis/exocytosis (Endo/Exo) ratio was significantly decreased from 57 ± 8% to 27 ± 5% at <4 vs. >11 min (p <0.01, $n = 10$). In contrast to the exocytosis-coupled endocytosis, ADP-induced endocytosis was independent of the whole-cell dialysis of dynPRD at 5 vs. 16 min (*lower traces*). On average, ADP-induced endocytosis were −93 ± 10 fF and −115 ± 14 fF, after break-in for <4 vs. >11 min, respectively ($n = 10$). (*B*) ADP-induced endocytosis is independent of GTP. (*Upper left*) During whole-cell dialysis of 2 mM GTPγS the ADP-induced endocytosis was intact, as compared at 3 vs. 12 min. (*Upper right*) Statistically, ADP-induced endocytosis were −97 ± 12 fF and −94 ± 11 fF at <3 min and >9 min, respectively ($n = 8$). (*Lower left*) Whole-cell dialysis of GTPγS blocked depolarization (Vm from −80 to 0 mV for 100 ms)-induced Ca^{2+} currents (I_m). Comparing the control neuron with Ca^{2+} currents induced by a 100-ms pulse from −80 to 0 mV, the Ca^{2+} current was blocked in another neuron by intracellular dialysis with GTPγS. The two neurons were from same batch. (*Lower right*) Four minutes after break-in, the Ca^{2+} currents were 1202 ± 180 pA and 110 ± 19 pA in control ($n = 6$) and GTPγS ($n = 8$) dialyzed neurons, respectively.

GTP hydrolysis for normal function. Whole-cell dialysis of GTPγS, a nonhydrolyzed form of GTP, did not affect ADP-induced endocytosis (Fig. 4 B), indicating that GTP hydrolysis was not required. These data suggest that ADP-induced endocytosis is completely dynamin-independent.

GPCR-induced endocytosis visualized by confocal single vesicle imaging

To confirm that the ADP-induced Cm change is indeed a signal of endocytosis, we adopted an imaging approach to visualize the endocytotic events with the fluorescent styryl dye FM2-10 (17,46,47). Incubating neurons in 0.1 mM FM2-10 and 0.1 mM ADP for 3 min resulted in a significant increase in the number of intracellular FM spots (Fig. 5), which are single vesicles loaded with FM2-10 (17). This was confirmed by the fact that few FM spots were observed if ADP was omitted during the FM2-10 incubation (control). The average number of FM spots (152 ± 39) and maximum ΔCm (-118 ± 17 fF) induced by 0.1 mM ADP for 3 min were consistent, assuming 0.5 fF per vesicle (142 nm in
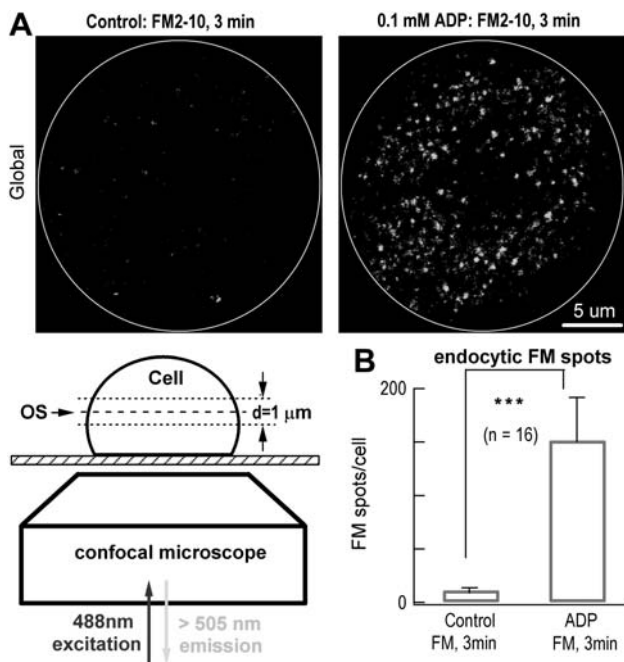
FIGURE 5 ADP-induced endocytosis measured by FM imaging. (A) ADP-induced endocytosis detected by FM2-10 imaging of single vesicle-like spots in single neurons. A representative neuron (*left panel*, control) was treated with 0.1 mM FM alone for 3 min at 37°C, and few FM spots appeared. Another representative neuron (*right panel*, ADP) was treated with 0.1 mM FM + 0.1 mM ADP for 3 min at 37°C, and a substantial number of FM spots appeared. The cell surfaces are marked as white cycles. Lower left is the protocol of FM imaging with 1-μm thick single optical slices (OS). The global FM image in panel A is a projection of 20 OSs from top to bottom of the cell. (B) Statistics of experiments of panel A. In the absence and presence of ADP, the numbers of FM spots were 11 ± 2 and 152 ± 39/cell, respectively ($n = 16$, $p < 0.01$).

diameter) (48). However, because some of the FM dyes might accumulate in intracellular organelles (i.e., lysosomes) during the 3 min, FM spots may not be an accurate measure of endocytotic vesicle numbers. Nevertheless, this experiment confirms that the ADP-induced Cm signal is a measure of ADP-induced endocytosis.

P2Y is internalized by the ADP-induced endocytosis

Ligand-induced endocytosis may or may not reflect the internalization of the receptor of the binding ligand (6,49). To determine whether P2Y is internalized by ADP-induced endocytosis, we expressed GFP-labeled P2Y1 in DRG neurons (Fig. 6 A) as well as in HEK293 cells (Fig. 6 B). Application of ADP for 20 min induced a dramatic translocation of the GFP fluorescence/P2Y1 from periphery to medulla, indicating internalization of P2Y1 via ADP-induced endocytosis. In contrast to ADP-induced endocytosis visualized as individual FM spots after 3 min FM incubation, no intracellular fluorescent spots were visible after 3 min ADP stimulation in GFP-P2Y labeled cells (data not shown). Instead, >10 min was required to visualize ADP-induced fluorescent structures. These intracellular structures might be accumulated GFP-labeled P2Y1 on organelles, which are much larger than endocytotic vesicles (Fig. 6). Possible interpretation for the differences between images measured by FM2-10 and GFP-labeling after ADP-induced endocytosis are presented in the Discussion.

DISCUSSION

In this work, we have recorded the temporal kinetics of endocytotic vesicles induced by a ligand binding to a GPCR. We demonstrated that i), the time constant of the ligand-induced endocytosis was 1.7 s; ii), ADP-induced endocytosis was dependent on nonspecific antagonists against the ADP receptor, phosphorylation and clathrin, but independent of dynamin; and iii), the ADP receptor P2Y was internalized by ADP-induced endocytosis.

Timing of GPCR-mediated endocytosis

The kinetics of stimulus-induced endocytosis is essential for understanding cell function and has been debated over 3 decades (10,17,50–54). Most previous studies in real-time assay concerned exocytosis-coupled endocytosis (17,26,46, 47,55). Here, we used real-time Cm recording to determine the kinetics of GPCR-coupled endocytosis. The 1.7-s time constant of ADP-induced endocytosis (at 24°C) provides the first example of a temporal profile from the vast GPCR family. Because the time resolution of Cm (in the ms range) is capable of measuring even faster changes, the time constant of 1.7 ± 0.2 s can be taken as accurate.
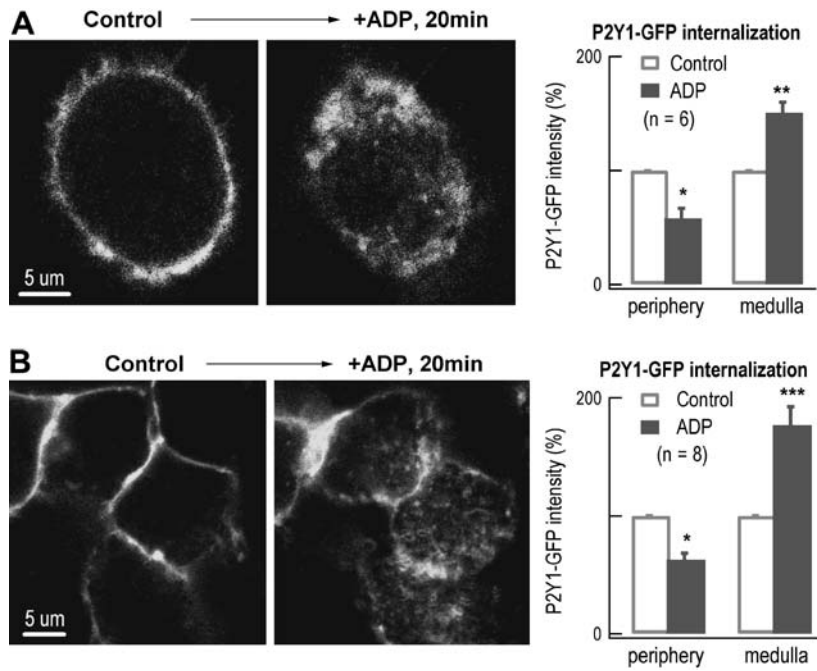
FIGURE 6 Evidence for internalization of P2Y1 receptors by ADP-induced endocytosis. (*A*) P2Y1 receptor internalization by ADP stimulation in transfected DRG neurons. In an optic slice (1 μm thick) of a representative transfected DRG neuron, the P2Y1-GFP receptors were overexpressed on the cell surface (*left panel*). Twenty minutes after applying ADP, another optical slice was taken at the same position of the cell. The P2Y1-GFP fluorescence translocated from the periphery toward the medulla (*middle panel*). Statistically, compared with their initial GFP-intensities, the GFP fluorescence was decreased by 42 $\pm$ 9% on the cell surface (within 2 μm from the surface) and increased by 51 $\pm$ 9% in the medulla after ADP stimulation ($n = 6$, *right panel*). (*B*) P2Y1 receptor internalization by ADP stimulation in transfected HEK293 cells. In an optic slice (1 μm thick) of the HEK293 cells, the P2Y1-GFP receptors were overexpressed on the cell surface (*left panel*). Twenty minutes after applying ADP, another optical slice was taken at the same position of the cells. The P2Y1-GFP fluorescence translocated toward the medulla after applying ADP for 20 min (*middle panel*). Statistically, the GFP fluorescence was decreased by 37 $\pm$ 6% on the cell surface and increased by 77 $\pm$ 16% in the medulla after ADP stimulation ($n = 8$, *right panel*).

Compared to the fast Ca^{2+}-dependent exocytosis, which occurs with a delay of <1 ms in synapses (1), the GPCR-mediated endocytosis is relative slow. Many steps are involved in LRB-induced endocytosis, including the binding between ligand and receptor, activation of the receptor, phosphorylation of the intracellular C-terminal of the receptor, β-arrestin activation, and clathrin-dependent endocytosis. These classic receptor-mediated steps apply to ADP-induced P2Y internalization in the DRG soma (Fig. 3). Future work will identify the time-limiting step in the LRB-induced signal pathway of endocytosis.

Dynamin independence of P2Y-induced endocytosis

We demonstrated that the signal pathway involved in ADP-induced endocytosis includes activation of the receptor, the Gi protein, phosphorylation, and clathrin (Fig. 3), these findings of the P2Y signaling, except the role of dynamin, are entirely consistent with literatures about GPCR-mediated endocytosis revealed by immunochemistry and biochemistry in neurons and other cell types. However, one of our interesting findings in the receptor signaling pathway is that ADP-induced endocytosis is dynamin-independent (Fig. 4). Most known receptor-mediated endocytosis in many cell types including neurons require dynamin (4–9), except for the dopaminergic D2-receptor (56). However, there are two types of exocytosis-coupled-endocytosis in the same DRG neurons. The slow endocytosis after Ca^{2+}-dependent exocytosis is dynamin-dependent, whereas the rapid endocytosis after Ca^{2+}-independent but voltage-dependent secretion, termed CIVDS-RE, is dynamin-independent (17). In this respect, the P2Y-mediated endocytosis shares the dynamin

independency of CIVDS-RE. In addition, again like CIVDS-RE, no $[Ca^{2+}]_i$ increase is associated with P2Y-mediated endocytosis (Fig. 2). Future work should address the mechanisms underlining dynamin-independent ADP-induced endocytosis.

ADP-induced endocytosis and internalization of P2Y receptors visualized by confocal imaging

To visualize ADP-induced endocytosis in the DRG soma, we used two independent labeling techniques in living cells (FM dye and GFP). Confocal FM imaging can detect single endocytotic vesicles after 3 min FM labeling in the soma (Fig. 5). However, despite the ability to label P2Y on the plasma membrane and on some large intracellular structures (in the 5 μm range; see Fig. 6) 20 min after ADP stimulation, single endocytotic vesicle images (in the 0.2 μm range) could not be obtained by GFP-labeling. In contrast, FM2-12 confocal image can visualize single endocytotic vesicles as individual FM spots (Fig. 5). Thus, confocal FM (but not GFP) imaging is a useful technique to study single vesicle traffic in living cells.

REFERENCES

1. Augustine, G. J., M. P. Charlton, and S. J. Smith. 1987. Calcium action in synaptic transmitter release. *Annu. Rev. Neurosci.* 10:633–693.

2. Katz, B. 1969. The Release of Neural Transmitter Substances. Liverpool University Press.

3. Rockman, H. A., W. J. Koch, and R. J. Lefkowitz. 2002. Seven-transmembrane-spanning receptors and heart function. *Nature.* 415:206–212.

4. Ferguson, S. S. 2001. Evolving concepts in G protein-coupled receptor endocytosis: the role in receptor desensitization and signaling. *Pharmacol. Rev.* 53:1–24.

5. Conner, S. D., and S. L. Schmid. 2003. Regulated portals of entry into the cell. *Nature.* 422:37–44.

6. Man, H. Y., J. W. Lin, W. H. Ju, G. Ahmadian, L. Liu, L. E. Becker, M. Sheng, and Y. T. Wang. 2000. Regulation of AMPA receptor-mediated synaptic transmission by clathrin-dependent receptor internalization. *Neuron.* 25:649–662.

7. Maxfield, F. R., and T. E. McGraw. 2004. Endocytic recycling. *Nat. Rev. Mol. Cell Biol.* 5:121–132.

8. von Zastrow, M. 2003. Mechanisms regulating membrane trafficking of G protein-coupled receptors in the endocytic pathway. *Life Sci.* 74:217–224.

9. Pelkmans, L., E. Fava, H. Grabner, M. Hannus, B. Habermann, E. Krausz, and M. Zerial. 2005. Genome-wide analysis of human kinases in clathrin- and caveolae/raft-mediated endocytosis. *Nature.* 436:78–86.

10. Ryan, T. A., S. J. Smith, and H. Reuter. 1996. The timing of synaptic vesicle endocytosis. *Proc. Natl. Acad. Sci. USA.* 93:5567–5571.

11. Richards, D. A., C. Guatimosim, and W. J. Betz. 2000. Two endocytic recycling routes selectively fill two vesicle pools in frog motor nerve terminals. *Neuron.* 27:551–559.

12. Kublaoui, B., J. Lee, and P. F. Pilch. 1995. Dynamics of signaling during insulin-stimulated endocytosis of its receptor in adipocytes. *J. Biol. Chem.* 270:59–65.

13. Holman, G. D., and I. V. Sandoval. 2001. Moving the insulin-regulated glucose transporter GLUT4 into and out of storage. *Trends Cell Biol.* 11:173–179.

14. Chowdhury, H. H., M. Kreft, and R. Zorec. 2002. Rapid insulin-induced exocytosis in white rat adipocytes. *Pflugers Arch.* 445:352–356.

15. Chowdhury, H. H., S. Grilc, and R. Zorec. 2005. Correlated ATP-induced changes in membrane area and membrane conductance in single rat adipocytes. *Ann. N. Y. Acad. Sci.* 1048:281–286.

16. Smith, C., and E. Neher. 1997. Multiple forms of endocytosis in bovine adrenal chromaffin cells. *J. Cell Biol.* 139:885–894.

17. Zhang, C., W. Xiong, H. Zheng, L. Wang, B. Lu, and Z. Zhou. 2004. Calcium- and dynamin-independent endocytosis in dorsal root ganglion neurons. *Neuron.* 42:225–236.

18. Marmorstein, A. D., C. Zurzolo, A. Le Bivic, and E. Rodriguez-Boulan. 1998. Cell surface biotinylation techniques and determination of protein polarity. *In* Cell Biology: A Laboratory Handbook, 2nd Ed. J. E. Celis, editor. Academic Press, San Diego, CA. 341.

19. Lu, Z., J. T. Murray, W. Luo, H. Li, X. Wu, H. Xu, J. M. Backer, and Y. G. Chen. 2002. Transforming growth factor beta activates Smad2 in the absence of receptor endocytosis. *J. Biol. Chem.* 277:29363–29368.

20. Ahmadian, G., W. Ju, L. Liu, M. Wyszynski, S. H. Lee, A. W. Dunah, C. Taghibiglou, Y. Wang, J. Lu, T. P. Wong, M. Sheng, and Y. T. Wang. 2004. Tyrosine phosphorylation of GluR2 is required for insulin-stimulated AMPA receptor endocytosis and LTD. *EMBO J.* 23:1040–1050.

21. Lindau, M., and E. Neher. 1988. Patch-clamp techniques for time-resolved capacitance measurements in single cells. *Pflugers Arch.* 411:137–146.

22. Artalejo, C. R., A. Elhamdani, and H. C. Palfrey. 2002. Sustained stimulation shifts the mechanism of endocytosis from dynamin-1-dependent rapid endocytosis to clathrin- and dynamin-2-mediated slow endocytosis in chromaffin cells. *Proc. Natl. Acad. Sci. USA.* 99:6358–6363.

23. Tse, A., F. W. Tse, W. Almers, and B. Hille. 1993. Rhythmic exocytosis stimulated by GnRH-induced calcium oscillations in rat gonadotropes. *Science.* 260:82–84.

24. Bao, L., S. X. Jin, C. Zhang, L. H. Wang, Z. Z. Xu, F. X. Zhang, L. C. Wang, F. S. Ning, H. J. Cai, J. S. Guan, H. S. Xiao, Z. Q. Xu, C. He, T. Hokfelt, Z. Zhou, and X. Zhang. 2003. Activation of delta opioid receptors induces receptor insertion and neuropeptide secretion. *Neuron.* 37:121–133.

25. Maruyama, Y., G. Inooka, Y. X. Li, Y. Miyashita, and H. Kasai. 1993. Agonist-induced localized Ca^{2+} spikes directly triggering exocytotic secretion in exocrine pancreas. *EMBO J.* 12:3017–3022.

26. Sun, J. Y., X. S. Wu, and L. G. Wu. 2002. Single and multiple vesicle fusion induce different rates of endocytosis at a central synapse. *Nature.* 417:555–559.

27. von Gersdorff, H., and G. Matthews. 1994. Inhibition of endocytosis by elevated internal calcium in a synaptic terminal. *Nature.* 370:652–655.

28. Zhang, C., and Z. Zhou. 2002. Ca^{2+}-independent but voltage-dependent secretion in mammalian dorsal root ganglion neurons. *Nat. Neurosci.* 5:425–430.

29. Huang, L. Y., and E. Neher. 1996. Ca^{2+}-dependent exocytosis in the somata of dorsal root ganglion neurons. *Neuron.* 17:135–145.

30. Moriyama, T., T. Iida, K. Kobayashi, T. Higashi, T. Fukuoka, H. Tsumura, C. Leon, N. Suzuki, K. Inoue, C. Gachet, K. Noguchi, and M. Tominaga. 2003. Possible involvement of P2Y2 metabotropic receptors in ATP-induced transient receptor potential vanilloid receptor 1-mediated thermal hypersensitivity. *J. Neurosci.* 23:6058–6062.

31. Yu, X., K. L. Duan, C. F. Shang, H. G. Yu, and Z. Zhou. 2004. Calcium influx through hyperpolarization-activated cation channels (I(h) channels) contributes to activity-evoked neuronal secretion. *Proc. Natl. Acad. Sci. USA.* 101:1051–1056.

32. Krzan, M., M. Stenovec, M. Kreft, T. Pangrsic, S. Grilc, P. G. Haydon, and R. Zorec. 2003. Calcium-dependent exocytosis of atrial natriuretic peptide from astrocytes. *J. Neurosci.* 23:1580–1583.

33. Zhou, Z., S. Misler, and R. H. Chow. 1996. Rapid fluctuations in transmitter release from single vesicles in bovine adrenal chromaffin cells. *Biophys. J.* 70:1543–1552.

34. Wu, B., Y. M. Wang, W. Xiong, L. H. Zheng, C. L. Fu, I. C. Bruce, C. Zhang, and Z. Zhou. 2005. Optimization of a multi-channel puffer system for rapid delivery of solutions during patch-clamp experiments. *Front. Biosci.* 10:761–767.

35. Ralevic, V., and G. Burnstock. 1998. Receptors for purines and pyrimidines. *Pharmacol. Rev.* 50:413–492.

36. Neves, G., A. Gomis, and L. Lagnado. 2001. Calcium influx selects the fast mode of endocytosis in the synaptic terminal of retinal bipolar cells. *Proc. Natl. Acad. Sci. USA.* 98:15282–15287.

37. Xia, J., H. J. Chung, C. Wihler, R. L. Huganir, and D. J. Linden. 2000. Cerebellar long-term depression requires PKC-regulated interactions between GluR2/3 and PDZ domain-containing proteins. *Neuron.* 28:499–510.

38. Schutze, S., T. Machleidt, D. Adam, R. Schwandner, K. Wiegmann, M. L. Kruse, M. Heinrich, M. Wickel, and M. Kronke. 1999. Inhibition of receptor internalization by monodansylcadaverine selectively blocks p55 tumor necrosis factor receptor death domain signaling. *J. Biol. Chem.* 274:10203–10212.

39. Damke, H., T. Baba, D. E. Warnock, and S. L. Schmid. 1994. Induction of mutant dynamin specifically blocks endocytic coated vesicle formation. *J. Cell Biol.* 127:915–934.

40. Marks, B., M. H. Stowell, Y. Vallis, I. G. Mills, A. Gibson, C. R. Hopkins, and H. T. McMahon. 2001. GTPase activity of dynamin and resulting conformation change are essential for endocytosis. *Nature.* 410:231–235.

41. McMahon, H. T. 1999. Endocytosis: an assembly protein for clathrin cages. *Curr. Biol.* 9:R332–R335.

42. Artalejo, C. R., J. R. Henley, M. A. McNiven, and H. C. Palfrey. 1995. Rapid endocytosis coupled to exocytosis in adrenal chromaffin cells involves Ca2+, GTP, and dynamin but not clathrin. *Proc. Natl. Acad. Sci. USA.* 92:8328–8332.

43. Wang, Y. T., and D. J. Linden. 2000. Expression of cerebellar long-term depression requires postsynaptic clathrin-mediated endocytosis. *Neuron*. 25:635–647.

44. Masur, S. K., Y. T. Kim, and C. F. Wu. 1990. Reversible inhibition of endocytosis in cultured neurons from the *Drosophila* temperature-sensitive mutant shibirets1. *J. Neurogenet*. 6:191–206.

45. Palfrey, H. C., and C. R. Artalejo. 2003. Secretion: kiss and run caught on film. *Curr. Biol*. 13:R397–R399.

46. Betz, W. J., and J. K. Angleson. 1998. The synaptic vesicle cycle. *Annu. Rev. Physiol*. 60:347–363.

47. Sankaranarayanan, S., and T. A. Ryan. 2000. Real-time measurements of vesicle-SNARE recycling in synapses of the central nervous system. *Nat. Cell Biol*. 2:197–204.

48. Zhang, X., K. Aman, and T. Hokfelt. 1995. Secretory pathways of neuropeptides in rat lumbar dorsal root ganglion neurons and effects of peripheral axotomy. *J. Comp. Neurol*. 352:481–500.

49. Gad, H., P. Low, E. Zotova, L. Brodin, and O. Shupliakov. 1998. Dissociation between Ca^{2+}-triggered synaptic vesicle exocytosis and clathrin-mediated endocytosis at a central synapse. *Neuron*. 21:607–616.

50. Ceccarelli, B., W. P. Hurlbut, and A. Mauro. 1973. Turnover of transmitter and synaptic vesicles at the frog neuromuscular junction. *J. Cell Biol*. 57:499–524.

51. Heuser, J. E., and T. S. Reese. 1973. Evidence for recycling of synaptic vesicle membrane during transmitter release at the frog neuromuscular junction. *J. Cell Biol*. 57:315–344.

52. Hsu, S. F., and M. B. Jackson. 1996. Rapid exocytosis and endocytosis in nerve terminals of the rat posterior pituitary. *J. Physiol*. 494:539–553.

53. Klingauf, J., E. T. Kavalali, and R. W. Tsien. 1998. Kinetics and regulation of fast endocytosis at hippocampal synapses. *Nature*. 394:581–585.

54. Gandhi, S. P., and C. F. Stevens. 2003. Three modes of synaptic vesicular recycling revealed by single-vesicle imaging. *Nature*. 423:607–613.

55. Lindau, M., and W. Almers. 1995. Structure and function of fusion pores in exocytosis and ectoplasmic membrane fusion. *Curr. Opin. Cell Biol*. 7:509–517.

56. Vickery, R. G., and M. von Zastrow. 1999. Distinct dynamin-dependent and -independent mechanisms target structurally homologous dopamine receptors to different endocytic membranes. *J. Cell Biol*. 144:31–43.